ChemistrySelect

ChemistrySelect
Chemistry Europe
European Chemical Societies Publishing

RESEARCH ARTICLE OPEN ACCESS

Enhanced Manganese Uptake by BTCA-Functionalized Lignocellulosic Felts

Dario Lacalamita[1,2] | Chiara Mongioví[1,3] | Nadia Morin-Crini[1] | Bernard Martel[4] | Jean-Noël Staelens[4] | Gilles Chanet[5] | Marina Raschetti[6] | Vincent Placet[7] | Xavier Gabrion[7] | Cesare Cosentino[7] | Grégorio Crini[1]

[1]UMR 6249 Chrono-environnement, Université Marie et Louis Pasteur, Besançon, France | [2]Dipartimento di Chimica, Università degli Studi di Bari "Aldo Moro", Bari, Italy | [3]Istituto per i Processi Chimico-Fisici, National Research Council, Bari, Italy | [4]UMR 8207-UMET-Unité Matériaux et Transformations, CNRS, INRAE, Université de Lille, Lille, France | [5]Eurochanvre, Arc-les-Gray, France | [6]SUPMICROTECH, CNRS, Institut FEMTO-ST, Université Marie et Louis Pasteur, Besançon, France | [7]Istituto di Chimica e Biochimica G. Ronzoni, Milano, Italy

Correspondence: Dario Lacalamita (dario.lacalamita@uniba.it) | Chiara Mongioví (c.mongiovi91@gmail.com) | Grégorio Crini (gregorio.crini@umlp.fr)

Received: 16 March 2026 | **Revised:** 8 April 2026 | **Accepted:** 13 April 2026

Keywords: butanetetracarboxylic acid | cellulose | flax | hemp | manganese

ABSTRACT

Lignocellulosic felts derived from hemp and flax were investigated as sustainable biosorbents for manganese ions removal from aqueous solutions, both in their native form and after functionalization through 1,2,3,4-butanetetracarboxylic acid (BTCA) grafting. Batch experiments were conducted to assess the influence of initial metal concentration, adsorbent dosage, pH, and ionic strength on biosorption performance. BTCA modification significantly enhanced Mn^{2+} uptake, with flax-based felts outperforming hemp due to their higher α-cellulose content, finer fiber morphology, and larger effective surface area. Mn^{2+} removal increased with adsorbent dosage and reached its maximum at pH values promoting deprotonation of BTCA carboxyl groups, confirming a complexation-driven mechanism. Increasing the solution ionic strength (0.1-0.5 M NaCl) reduced removal efficiency by competitive Na^+ interactions with cellulose, hemicellulose, and BTCA-derived -COO^- groups, though modified felts maintained superior performance. Adsorption isotherm modelling revealed distinct behaviors among materials: native felts fit moderately well to the Langmuir model, while BTCA-modified flax showed excellent agreement with Langmuir and Dubinin–Radushkevich models. The mean free energy of 18 kJ mol^{-1} confirmed chemisorption via metal-carboxylate coordination as the dominant mechanism. Overall, BTCA-modified flax felts emerged as highly effective and environmentally friendly biosorbents, offering strong potential for Mn^{2+} removal in industrial wastewater treatment applications.

1 | Introduction

Manganese, together with Iron, frequently occurs in water sources used for drinking water supply, with the former generally present at much lower concentrations [1–3]. Both elements occur naturally in soil and in most surface- and groundwater sources, but they may also originate from human activities [4–9]. In 2023, manganese was included in the list of Critical Raw Materials of the European Union, highlighting its strategic importance and supply vulnerability. South Africa and China currently account for the largest share of global manganese production, with approximately 29% and 58%, respectively [10]. This classification further emphasizes the need for sustainable management and recovery strategies for this element.

Furthermore, Mn is an essential element for many living organisms due to its role in enzymatic functions. It is considered one of the least toxic trace elements for humans, with diet being the primary source of exposure [11–13]. However, manganese levels in drinking water remain a topic of ongoing debate. High

manganese concentrations have been reported in occupational environments such as manganese mines, ore-processing plants, dry-cell battery manufacturing facilities, and ferromanganese production plants, where airborne concentrations may range from 10 to 250 mg/m^3 [14–16].

While manganese homeostasis is generally well regulated when exposure occurs via ingestion, inhalation represents a critical pathway. Inhaled Mn can bypass hepatic regulation, reach the brain directly, and accumulate in specific regions of the central nervous system, potentially leading to neurotoxic effects such as impairments in memory, attention, and motor functions [14–18]. Young children are particularly vulnerable to elevated manganese exposure [19]. Moreover, radiolabeled manganese studies have shown that the metal is slowly taken up and retained in neural tissues [20, 21].

In France, the quality standards for drinking water set maximum concentrations of 0.2 mg/L for iron and 0.05 mg/L for manganese. Unlike iron, which has an emission concentration limit of 5 mg/L combined with Al, no regulatory limit exists for Mn in industrial wastewater [22]. As a result, this element is discharged into rivers at non-negligible concentrations, contaminating water bodies used as drinking-water sources.

Nevertheless, several companies, such as those in the surface treatment sector, are concerned by the issue of metallic substances present in their emissions, some of which are classified as hazardous substances or priority hazardous substances [23–25]. Although Manganese does not fall into these categories, studies conducted by Crini and coworkers have shown that Mn concentration released from the surface-treatment industry can be relatively high [24]. Conventional treatment methods rely mainly on chemical precipitation via alkaline agents such as lime, resulting in the formation of metal hydroxides [26]. If emission standards are met, treated effluents are discharged into the environment.

In France, the recently introduced Plan EAU 2030 requires additional efforts from industries to further reduce contaminant discharges into the environment [27–29]. Complementary treatment methods such as ion-exchange resins and reverse osmosis exist, but they are costly for small industrial facilities. Resins are sensitive and require upstream protection with activated-carbon filters [30, 31]. There is therefore a need for simple, efficient, environmentally friendly, and economically sustainable solutions for small-scale industries [32].

In this context, biosorption using lignocellulosic materials has emerged as a promising alternative for metal removal from aqueous media [33, 34]. Lignocellulosic felts derived from natural fibers combine renewability, low cost, mechanical robustness, and a high density of functional groups, such as hydroxyl and carboxyl moieties, capable of interacting with metal ions [35–38]. Hemp and flax fibers, in particular, are attractive due to their high cellulose content, tunable surface chemistry, and availability from agricultural sources [39–43].

In this study, the potential of lignocellulosic felts derived from hemp and flax, as sustainable biosorbents for the removal of manganese ions (Mn^{2+}) from aqueous solutions, was investigated using the classical batch method. Native felts were compared with felts chemically modified through grafting with 1,2,3,4-butanetetracarboxylic acid (BTCA) to enhance the density of carboxylic functional groups. Batch experiments were conducted to assess the influence of initial metal concentration, adsorbent dosage, pH, and ionic strength on biosorption performance. The experimental data were modelled using common isotherm models such as Langmuir, Freundlich, Temkin, and Dubinin–Radushkevich (D–R).

2 | Results and Discussion

2.1 | Felt Characterization

The surface morphology of native and modified felts was examined by scanning electron microscopy (SEM), while structural changes were further investigated by solid-state NMR spectroscopy. SEM observations in Figure 1 revealed that both hemp and flax felts consisted of large fiber bundles interspersed with isolated single fibers. A BTCA coating was clearly visible on the surface of treated hemp and flax fibers. No significant morphological differences were observed between native hemp and flax felts; however, HEMPM exhibited a less smooth surface compared to untreated hemp, while FLAXM displayed a pronounced increase in surface roughness, indicative of a more effective grafting process. Overall, qualitative SEM analysis confirmed that chemical modification significantly altered the surface morphology and roughness of the fibers. In addition, upon their handling, treated samples displayed increased stiffness compared with the raw materials. As demonstrated by Welsh et al., polycarboxylic acids like citric acid and BTCA effectively improve the dimensional stability and stiffness of paper. Beyond paper science, these agents are industrially significant as formaldehyde-free alternatives for the durable press finishing of cotton and wool [44–46].

Elemental surface analysis (Figure S2) showed no substantial differences between hemp and flax before and after modification. Carbon and oxygen were the predominant elements detected on the fiber surfaces. Trace amounts of sodium, magnesium, aluminum, silicon, phosphorus, sulfur, chlorine, potassium, calcium, and chromium were also observed, likely originating from soil or fertilizer uptake and incorporation into the hemp and flax plant cell walls [47]. A detailed discussion of these mineral components has been reported elsewhere [48]. Potassium and calcium, in particular, are essential for plant metabolism and growth-related physiological processes, with calcium ions known to act as bridging agents between pectin molecules [49–52]. After chemical treatment, hemp and flax fibers exhibited the same elemental composition than native samples, with the additional presence of sodium, attributed to activation of the modified felts using an aqueous $NaHCO_3$ solution prior to use.

These findings were further supported by solid-state ^{13}C NMR analysis. The CP/MAS spectrum of native flax (Figure 2, top) displayed broad resonances between 50 and 110 ppm, characteristic of disordered cellulose and corresponding to the glucopyranose units of the raw fiber. In contrast, the spectrum of FLAXM showed additional signals, notably a broad band in the 170–180 ppm region assigned to carboxylic groups, confirming successful crosslinking with BTCA. This band (labeled a and d) corresponds

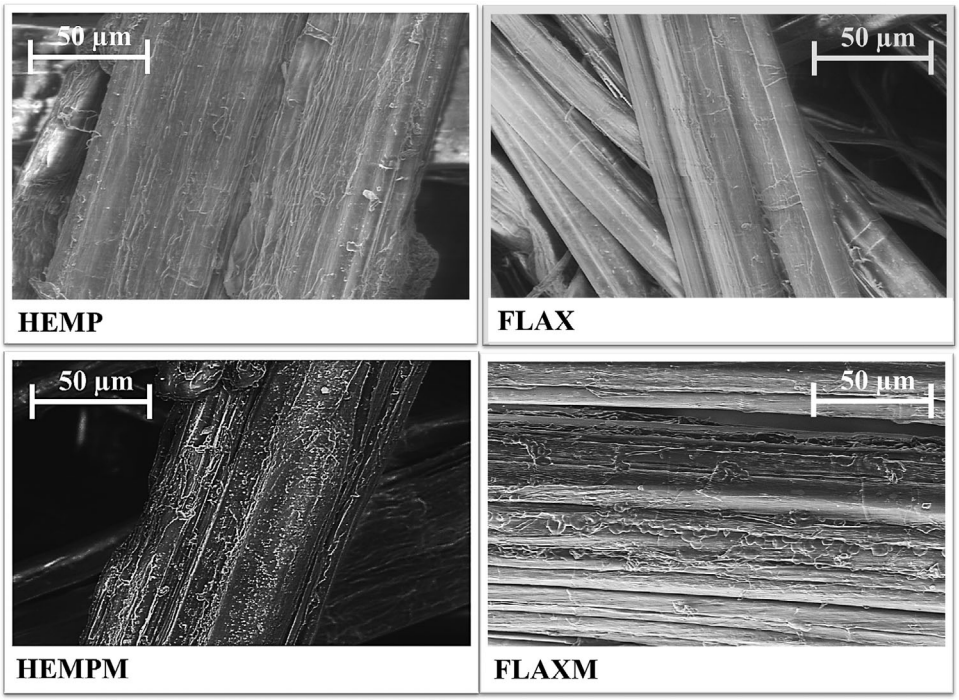

FIGURE 1 | Electron microscopy images of the felts surface. At the top of the figure, native felt fibers are depicted, while BTCA-grafted fibers are shown at the bottom.

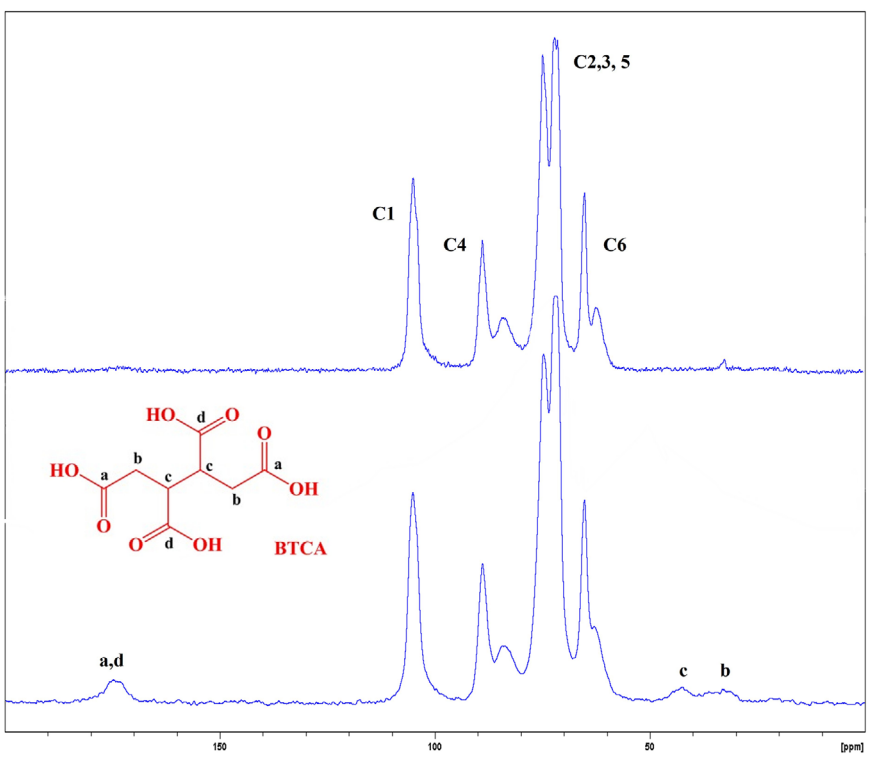

FIGURE 2 | Solid-state ^{13}C cross polarization magic angle spinning (CP-MAS) nuclear magnetic resonance spectra of the native flax felt (top), and BTCA-modified flax felt (bottom). The CPMAS for flax shows the peaks of disordered cellulose (C1–C6 broad signals attributable to the glucopyranose unit) in the range of 50–100 ppm. The spectrum of modified flax shows a large band between 170 and 180 ppm (peaks noted a and d) attributed to carboxylic groups and two other signals (labeled c and b) due to the cross-linking agent. These new peaks confirm the cross-linking reaction by the BTCA (see Figure **S1**).

TABLE 1 | Values of ion exchange capacity for the different materials.

Lignocellulosic sample	Ion exchange capacity (meq COOH per g)
HEMP	0.15 ± 0.02
HEMPM	1.3 ± 0.1
FLAX	0.64 ± 0.04
FLAXM	1.4 ± 0.1

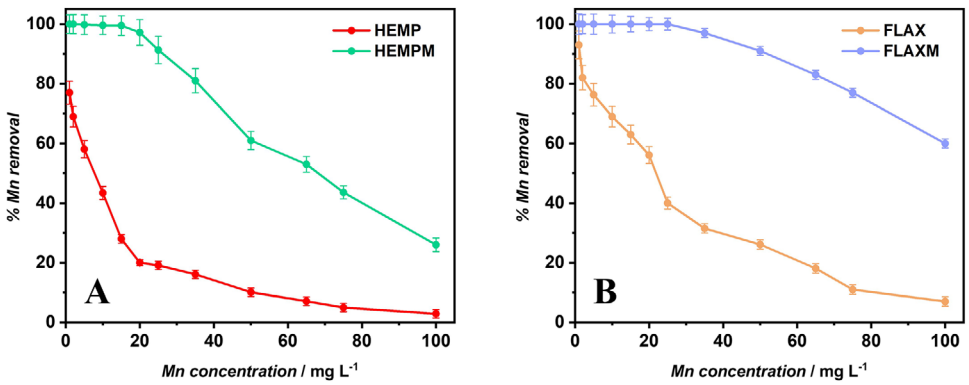

FIGURE 3 | Effect of the initial Mn concentration on the removal efficiency of hemp- and flax-based felts, in their native (HEMP, FLAX) and BTCA-modified (HEMPM, FLAXM) forms. (A) HEMP versus HEMPM; (B) FLAX versus FLAXM. Experimental conditions: adsorbent dose = 1 g; pH = 5; contact time = 1 h; temperature = 22 ± 1°C; volume of solution = 0.1 L.

to esterified and free carboxylic groups arising from BTCA present as both ester crosslinks and residual carboxylic acids. Additional resonances between 30 and 50 ppm (labeled b and c) were also attributed to the BTCA crosslinking agent. Similar spectra were obtained for modified hemp felts, in agreement with previously reported results [47] (Figure S3).

2.2 | Differences in Ion Exchange Capacity

The ion-exchange capacity (IEC) of hemp and flax felts was determined by pH-metric titration using the calcium acetate method, as previously described [53]. As summarized in Table 1, potentiometric titration revealed a substantial increase in the concentration of carboxylic groups after grafting. The IEC of hemp increased from 0.15 ± 0.02 meq g^{-1} for the native material (HEMP) to 1.3 ± 0.1 meq g^{-1} for the modified felt (HEMPM). Notably, native flax exhibited an IEC approximately four times higher than that of native hemp, with a value of 0.64 ± 0.04 meq g^{-1}. Following grafting, FLAXM reached an IEC of 1.4 ± 0.1 meq g^{-1}, representing the highest ion-exchange capacity among the felts investigated.

2.3 | Comparison Between the Lignocellulosic Felts for Mn Removal

Mn uptake was investigated using the batch method for the four different felts. Figure 3 illustrates the effect of the initial Mn concentration on the removal efficiency of the four investigated felts. In all cases, Mn removal decreases as the metal concentration increases, reflecting the progressive saturation of available biosorption sites. However, clear differences emerge between the unmodified felts (HEMP and FLAX) and those functionalized with BTCA (HEMPM and FLAXM). Among the natural materials, HEMP displays the lowest biosorption performance across the entire concentration range, with removal efficiencies dropping below 20% at concentrations above 20 mg L^{-1}. FLAX performs slightly better than HEMP, although it also exhibits a pronounced decline in removal at higher Mn levels. As reported by Mongioví et al., the flax-based felt provides a higher exchange surface area due to its finer fibers and higher α-cellulose content compared with hemp, which is consistent with the superior performance observed here [34]. Furthermore, the biosorption process is likely controlled by a combination of external mass transfer and diffusion within the porous fibrous structure, followed by interaction with active sites.

The BTCA modification significantly enhances the biosorption capacity of both fibers. HEMPM shows a marked improvement compared with the native hemp felt, maintaining removal efficiencies above 50% up to approximately 60 mg L^{-1} and displaying a more gradual decrease thereafter. FLAXM is the most effective adsorbent overall; its removal efficiency remains high across the full concentration range, and the decline with increasing Mn concentration is notably less severe than that observed for the other materials. The direct comparison between the modified felts (Figure 3) confirms that FLAXM outperforms HEMPM, indicating a stronger affinity toward Mn and a higher density of effective binding sites.

Overall, the results demonstrate that (i) BTCA grafting substantially increases the biosorption capacity of both hemp and flax

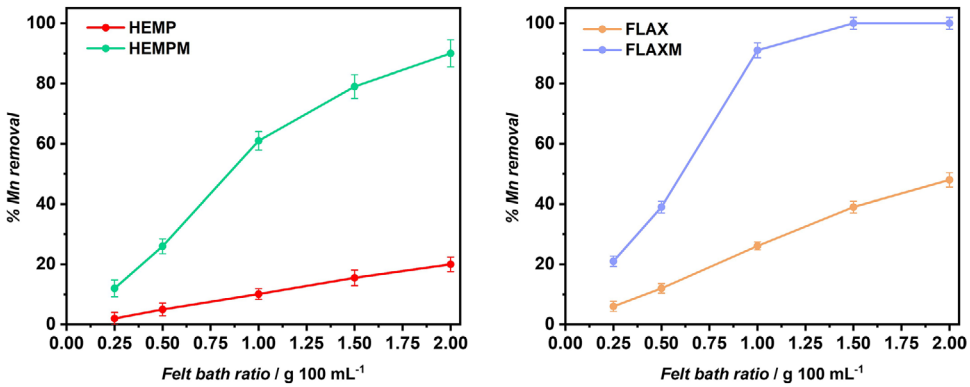

FIGURE 4 | Influence of the felt bath ratio on Mn removal for native (HEMP, FLAX) and BTCA-modified (HEMPM, FLAXM) felts. (left) HEMP versus HEMPM; (right) FLAX versus FLAXM. Increasing the felt dosage enhances Mn removal for all materials, with the modified felts showing the most pronounced improvement. Experimental conditions: initial Mn concentration = 50 mg L^{-1}; pH = 5; contact time = 1 h; temperature = 22 ± 1°C; volume of solution 0.1 L.

felts, (ii) flax inherently performs better than hemp, both before and after modification, and (iii) FLAXM represents the most efficient biosorbent for Mn removal among those evaluated.

2.4 | Effect of Adsorbent Dosage on Mn Removal Efficiency

Figure 4 shows the influence of the felt bath ratio on Mn removal for the unmodified and BTCA-modified felts. For all materials, the removal efficiency increases as the felt dosage increases, reflecting the higher number of available biosorption sites introduced into the system. However, the extent of this improvement varies substantially among the four felts. HEMP exhibits the lowest performance, with only a modest increase in Mn removal even at the highest tested dosage. FLAX performs better than HEMP, showing a more pronounced and nearly linear improvement as the felt bath ratio increases, in agreement with the higher surface accessibility and fiber fineness previously reported for flax-based felts.

The BTCA-modified materials display a markedly enhanced response to increasing dosage. HEMPM shows a strong, dose-dependent increase in Mn removal, reaching values above 80% at the highest felt bath ratio. FLAXM stands out as the most efficient adsorbent, achieving high removal efficiency even at low dosage and approaching quantitative Mn removal as the felt amount increases. The comparison between the modified felts clearly highlights that FLAXM consistently outperforms HEMPM, suggesting that the BTCA grafting is more effective on the flax substrate, likely due to its higher α-cellulose content and greater accessible surface area.

Overall, the results demonstrate that the adsorbent dosage is a key parameter governing Mn removal and that the combination of BTCA functionalization and flax-based structure provides the most effective configuration for maximizing biosorption performance.

2.5 | PH Influence on the Biosorption Process

Solution pH is a key parameter governing Mn removal, as it simultaneously affects metal speciation in solution and the degree of ionization of the functional groups present on the adsorbent surface. In this study, the influence of pH was evaluated within the 2–6 range, which corresponds to the typical pH values of effluents generated by the surface-treatment industry. At low pH (2–3), the surface of both hemp and flax felts is predominantly protonated, leading to strong electrostatic repulsion between positively charged functional groups and Mn^{2+} ions. This results in limited biosorption, particularly for the unmodified materials. The introduction of BTCA, however, significantly alters the surface chemistry of the felts: the grafted BTCA molecules contribute multiple carboxylic groups with pKa values of 3.43, 4.58, 5.85, and 7.16 (Figure 5A) [54, 55]. As the pH increases, these groups progressively deprotonate, generating negatively charged sites capable of strongly interacting with Mn^{2+} through electrostatic attraction and metal-carboxylate complexation. However, the pKa of the grafted COOH cannot be defined precisely because it is difficult to state that BTCA is esterified by one, two, or more of its carboxylic groups (Figure S1).

This sequential deprotonation mechanism provides a clear interpretation of the observed pH-dependent removal efficiency. Around pH 3, only the most acidic carboxyl group [pKa ≈ 3.43] begins to deprotonate, resulting in a limited but noticeable increase in Mn uptake. At pH 4–5, two additional carboxyl groups [pKa 4.58 and 5.85] become deprotonated, markedly enhancing the density of negatively charged biosorption sites. This leads to a significant improvement in Mn removal for the modified felts, which consistently outperform the natural ones (Figure 5B). By pH 6, the surface bears a high proportion of deprotonated carboxylates, maximizing electrostatic attraction and coordination with Mn^{2+}. In this condition, biosorption is governed predominantly by metal-carboxylate complexation, explaining the high efficiencies observed for BTCA-modified flax and hemp. Control experiments performed in the absence of adsorbent confirmed that no Mn removal occurred within the investigated pH range, excluding precipitation phenomena.

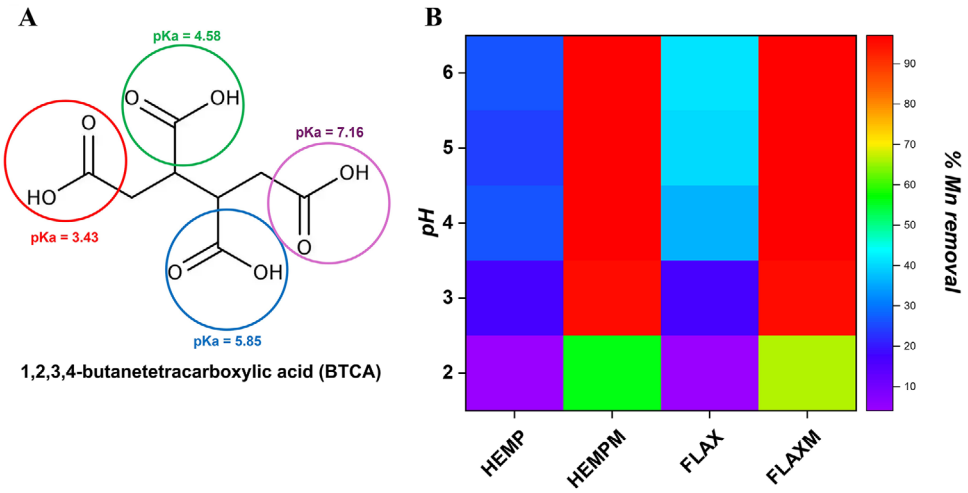

FIGURE 5 | (A) Chemical structure of 1,2,3,4-butanetetracarboxylic acid (BTCA) and its pKa; (B) effect of solution pH (2–6) on Mn removal by natural (HEMP, FLAX) and BTCA-modified (HEMPM, FLAXM) felts. Modified felts consistently show higher removal efficiency due to the progressive deprotonation of BTCA carboxyl groups and the resulting increase in negatively charged adsorption sites, which enhances electrostatic attraction and metal–carboxylate complexation with Mn^{2+}. Experimental conditions: adsorbent dose = 1 g; initial Mn concentration = 50 mg L^{-1}; contact time = 1 h; temperature = 22 ± 1°C; volume of solution = 0.1 L.

Overall, these results show that the pH-dependent ionization of BTCA carboxyl groups plays a central mechanistic role in Mn uptake: higher pH values increase the negative charge of the adsorbent surface, thereby promoting more efficient biosorption through a combination of electrostatic interactions and complex formation. This also accounts for the superior performance of BTCA-modified felts compared to their unmodified counterparts across the entire pH range investigated.

The pH-dependent protonation and deprotonation of surface functional groups not only governs Mn^{2+} adsorption but can also be exploited for desorption and material regeneration. In particular, the protonation of carboxylate groups under acidic conditions promotes the release of previously adsorbed Mn^{2+} ions, enabling the reuse of the biosorbent.

This mechanism was applied to evaluate the reusability of the BTCA-modified felts, as reported in the Supporting Information (Figure S4). Regeneration was performed using a dilute acidic solution, followed by rinsing and reuse in fresh Mn^{2+} solutions. The results demonstrate that both materials retain significant adsorption capacity over multiple cycles, with the modified flax felt exhibiting higher initial performance but a more pronounced decrease upon reuse, likely due to its lower mechanical resistance compared to hemp-based felts.

In summary, these findings confirm that the adsorption process is at least partially reversible and that the developed materials can be regenerated through simple pH adjustment, supporting their potential for practical applications.

2.6 | Ionic Strength Effect on Biosorption

To elucidate the contribution of BTCA carboxyl groups to Mn^{2+} binding, the effect of increasing ionic strength was investigated by adding NaCl at 0.1 M and 0.5 M. As shown in Figure 6, the presence of Na^+ progressively reduced Mn removal in all materials, although the magnitude of this effect differed significantly between native and BTCA-modified felts. For the unmodified HEMP felt, Mn removal decreased only slightly from 19 ± 1% in the absence of NaCl to 17 ± 1% at 0.1 M and 10 ± 1% at 0.5 M, reflecting the limited number of weakly acidic -OH groups

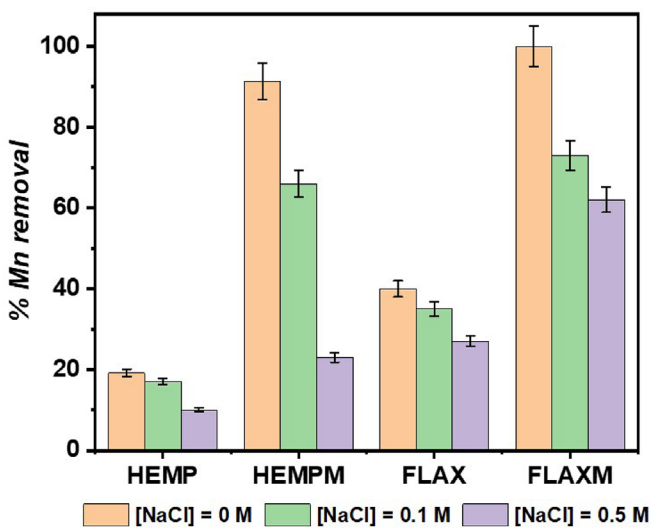

FIGURE 6 | Effect of ionic strength on Mn^{2+} removal by native and BTCA-modified hemp and flax felts. Percentage Mn removal (%) obtained for HEMP, HEMPM, FLAX, and FLAXM in solutions containing 0 M, 0.1 M, and 0.5 M NaCl. The progressive decrease in removal efficiency with increasing NaCl concentration highlights the competitive role of Na^+ ions, which screen or occupy the biosorption sites of lignocellulosic fibers and interact with the carboxylate groups introduced by BTCA grafting. Experimental conditions: initial Mn concentration = 50 mg L^{-1}; pH = 5; adsorbent dose = 1 g; contact time = 1 h; temperature = 22 ± 1°C; volume of solution = 0.1 L.

(from cellulose and hemicellulose) available for metal binding. In contrast, HEMPM showed markedly higher biosorption capacity under all conditions, removing 91 ± 5% of Mn in the absence of NaCl, 66 ± 3% at 0.1 M and 23 ± 1% at 0.5 M. A similar pattern was observed for FLAX and FLAXM. Native FLAX removed 40 ± 2%Mn at 0 M, decreasing to 35 ± 2% at 0.1 M and 27 ± 1% at 0.5 M, whereas FLAXM maintained the highest efficiencies across the series, falling from 100% at 0 M to 73 ± 4% at 0.1 M and 62 ± 3% at 0.5 M.

These trends clearly indicate that Na^+ competes with Mn^{2+} through electrostatic screening of negatively charged biosorption sites. In native fibers, Na^+ mainly shields the surface -OH groups, reducing their ability to interact with Mn^{2+}. In BTCA-modified felts, however, Na^+ can also interact directly with deprotonated $-COO^-$ groups, which are primarily responsible for strong complexation with Mn^{2+}. As ionic strength increases, Na^+ increasingly saturates these high-affinity sites, diminishing the driving force for Mn^{2+} complexation. According to the Le Chatelier principle, increasing the concentration of competing Na^+ shifts the ion-exchange equilibrium toward Na^+–COO^- association, thereby reducing Mn^{2+} uptake. This mechanism also explains the regeneration behavior of BTCA-modified felts, where Na^+ effectively displaces Mn^{2+} from carboxylate sites.

The sharper decline observed for HEMPM and FLAXM, therefore, confirms the dominant role of BTCA carboxylate groups in Mn^{2+} uptake and highlights the sensitivity of these functional groups to competitive cation effects.

2.7 | Adsorption Isotherms Modeling

A comprehensive investigation of the adsorbate-adsorbent equilibrium relationships for lignocellulosic felts was performed using the Langmuir, Freundlich, Temkin, and D–R isotherm models (Figure 7). The resulting trends indicate that multiple interaction mechanisms contribute to Mn^{2+} uptake, reflecting the heterogeneous chemical composition of the felts and complicating the interpretation of a single prevailing adsorption model.

The native HEMP exhibited the best linearity under the Langmuir formalism, suggesting monolayer adsorption on a relatively homogeneous distribution of active sites. The corresponding maximum adsorption capacity, Q_0, calculated from the Langmuir plot, was approximately 0.33 mg g^{-1}. A similar behavior was observed for native FLAX, although its higher Q_0 value of 0.83 mg g^{-1} indicates superior Mn^{2+} affinity, most likely due to the higher α-cellulose content and lower hemicellulose fraction of flax compared to hemp.

Unlike the native felts, HEMPM did not show a clear predominance of any of the four models. The poor exclusivity of the fit suggests that Mn^{2+} uptake occurs through multiple concurrent mechanisms, consistent with the introduction of BTCA carboxylate groups generating both specific complexation sites and residual native biosorption domains.

In contrast, FLAXM displayed remarkably good agreement with Langmuir, Temkin, and D–R models, indicating that BTCA modification led to a more uniform population of biosorption sites and enhanced Mn^{2+} affinity. Its Langmuir Q_0 reached 10.7 mg g^{-1}, about 13-fold higher than FLAX and nearly 3-fold higher than HEMPM, confirming the strong impact of BTCA functionalization. This substantial increase can be linked to flax's inherently higher α-cellulose content, which provides more accessible hydroxyl groups for BTCA crosslinking and thus more available $-COO^-$ binding sites.

The D-R model further supported the presence of strong interactions in FLAXM: the mean free energy (E) was 18.2 kJ mol^{-1}, significantly exceeding the 8 kJ mol^{-1} threshold typically associated with physisorption. This strongly suggests that Mn^{2+} uptake is dominated by chemisorption, most plausibly through coordination with BTCA-derived $-COO^-$ groups. Although E-values for the other felts also fall within the chemisorption domain, their weaker fit to the D–R model prevents definitive mechanistic conclusions (Table 2).

Finally, it is worth noting that structural differences, such as the higher thickness of HEMP (5 mm) compared to FLAX (3 mm), may influence BTCA penetration and internal accessibility of biosorption sites, contributing to the observed variability in the isotherm behaviors and complicating direct comparison between materials.

In addition to the linearized models commonly reported in the literature, non-linear regression analysis was performed to fit Langmuir, Freundlich, Temkin, and D–R isotherm models, in accordance with recent recommendations in the literature. The non-linear fitting results are reported in Figure 8, while the corresponding parameters are summarized in Table 3. The comparison between non-linear and linearized models highlights that, although the general trends are consistent, noticeable differences in the estimated parameters can be observed. In particular, non-linear fitting provides a more accurate description of the experimental data, especially at low and high concentration ranges, where linearization may introduce distortions due to error transformation.

For modified felts (HEMPM and FLAXM), all models exhibit a good agreement with the experimental data, confirming the well-defined biosorption behavior induced by BTCA functionalization. On the contrary, native felts (HEMP and FLAX) show a larger deviation between models, reflecting the more heterogeneous nature of the biosorption process.

The comparison between Tables 2 and 3 highlights the extent to which parameter estimation depends on the fitting approach, emphasizing the importance of non-linear regression for a more reliable interpretation of biosorption mechanisms.

It is interesting to note that even in the nonlinearized form, the mean free energy is greater than 8 kJ mol^{-1}, confirming a chemisorption behavior due to the presence of carboxylate moieties on the felts surface

Overall, from a physicochemical point of view, both isothermal representations show that the grafting process uniformed the surface. Indeed, the biosorption process results are repeatable with better fittings for grafted felts compared to non-modified felts. Nevertheless, the heterogeneous surface make complex

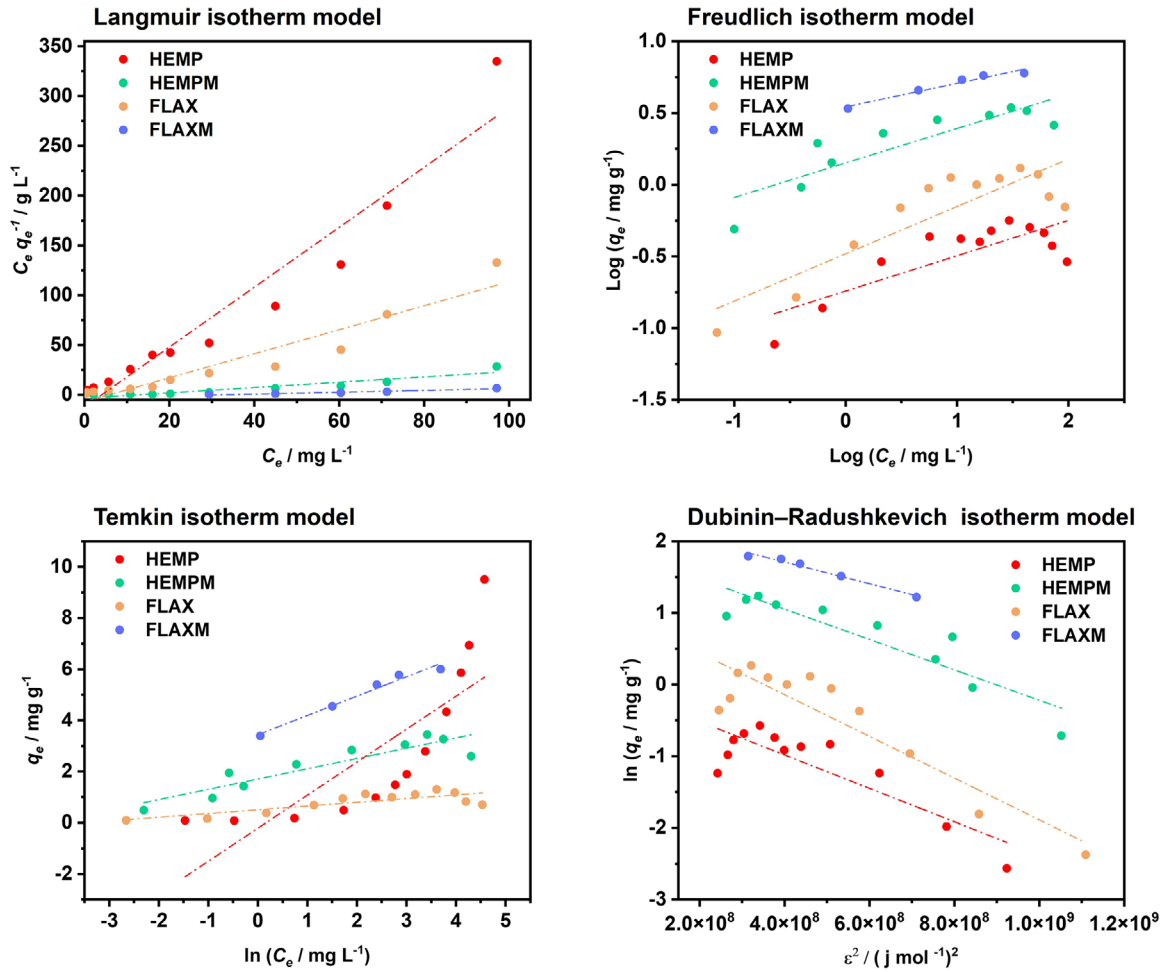

FIGURE 7 | Adsorption isotherms of Mn^{2+} on native (HEMP, FLAX) and BTCA-modified (HEMPM, FLAXM) lignocellulosic felts. Linearized plots according to the Langmuir, Freundlich, Temkin, and D–R models are shown. Experimental conditions: adsorbent dose = 1 g; pH = 5; contact time = 1 h; temperature = 22 ± 1°C; volume of solution = 0.1 L.

determines which biosorption process majorly occurs on the lignocellulosic felts.

2.8 | X-Ray Computed Nanotomography Reconstruction

To further support these observations, a surface investigation was conducted using x-ray computed nanotomography (nano-CT) on individual fibers extracted from the BTCA-modified flax felt, which exhibited the highest manganese concentrations among all samples. This technique allowed for nondestructive, three-dimensional visualization of the fiber morphology and the distribution of adsorbed Mn at the microscale. Figure 9 presents the reconstructed images of the flax fibers before biosorption (Figure 9A) and after exposure to manganese (Figure 9B–D), with manganese highlighted in red. The 3D reconstruction prior to biosorption confirms the SEM observations, revealing a highly rough surface, which may contribute to increased accessibility of reactive sites for functionalization. Following manganese biosorption, the nano-CT images show that manganese is primarily localized along the external surface of the fibers. This preferential surface localization can be explained by stronger interactions between manganese ions and the carboxylate groups introduced by BTCA, particularly in the regions most exposed to the solution. These findings indicate that biosorption occurs mainly at the fiber surface rather than within the bulk and strongly support a chemisorption-dominated mechanism, driven by the BTCA carboxyl groups.

2.9 | Performance Comparison of Biosorbents for Mn^{2+} Removal

To better contextualize the performance of the proposed materials, a comparison with recent low-cost biosorbents reported in the literature for metal removal is presented (Table 4). It should be noted that a direct comparison remains challenging due to the variability in experimental conditions, including pH, initial metal concentration, contact time, and adsorbent dosage, which strongly influence biosorption capacity and removal efficiency. Furthermore, Mn(II) biosorption is less studied than Pb or Cd.

Despite these differences, some general trends can be highlighted. Several lignocellulosic and waste-derived materials, such as *Phragmites australis*, corncob biomass, and tannic acid-functionalized cellulose, exhibit biosorption capacities ranging from approximately 6 to over 30 mg g^{-1}, often accompanied by

TABLE 2 | Isotherm parameters obtained from the linear modelling of the Mn^{2+} adsorption through native lignocellulosic (HEMP, FLAX) and BTCA-modified (HEMPM, FLAXM) felts.

	Freundlich isotherm model			Langmuir isotherm model			Temkin isotherm model			Dubinin–Radushkevich isotherm model			
HEMP	K_F (L mg^{-1})	n	R^2	K_L (L mg^{-1})	Q_0 (mg g^{-1})	R^2	K_T (L mol^{-1})	B_1	R^2	K_{D-R} (mol^2 J^{-2})	Q_0 (mg g^{-1})	E (kJ mol^{-1})	R^2
	0.18	4.1	0.62	0.25	0.33	0.93	0.85	1.3	0.60	2.3×10^{-9}	0.95	14.6	0.70
HEMPM	K_F (L mg^{-1})	n	R^2	K_L (L mg^{-1})	Q_0 (mg g^{-1})	R^2	K_T (L mol^{-1})	B_1	R^2	K_{D-R} (mol^2 J^{-2})	Q_0 (mg g^{-1})	E (kJ mol^{-1})	R^2
	1.40	4.2	0.74	0.08	3.80	0.88	70	0.4	0.81	2.1×10^{-9}	6.7	15.3	0.80
FLAX	K_F (L mg^{-1})	n	R^2	K_L (L mg^{-1})	Q_0 (mg g^{-1})	R^2	K_T (L mol^{-1})	B_1	R^2	K_{D-R} (mol^2 J^{-2})	Q_0 (mg g^{-1})	E (kJ mol^{-1})	R^2
	0.33	3.0	0.74	0.20	0.83	0.91	32.3	0.15	0.62	2.9×10^{-9}	2.8	13.1	0.82
FLAXM	K_F (L mg^{-1})	n	R^2	K_L (L mg^{-1})	Q_0 (mg g^{-1})	R^2	K_T (L mol^{-1})	B_1	R^2	K_{D-R} (mol^2 J^{-2})	Q_0 (mg g^{-1})	E (kJ mol^{-1})	R^2
	3.50	6.1	0.95	0.03	10.7	0.92	94.4	0.8	0.97	1.5×10^{-9}	10.0	18.2	0.97

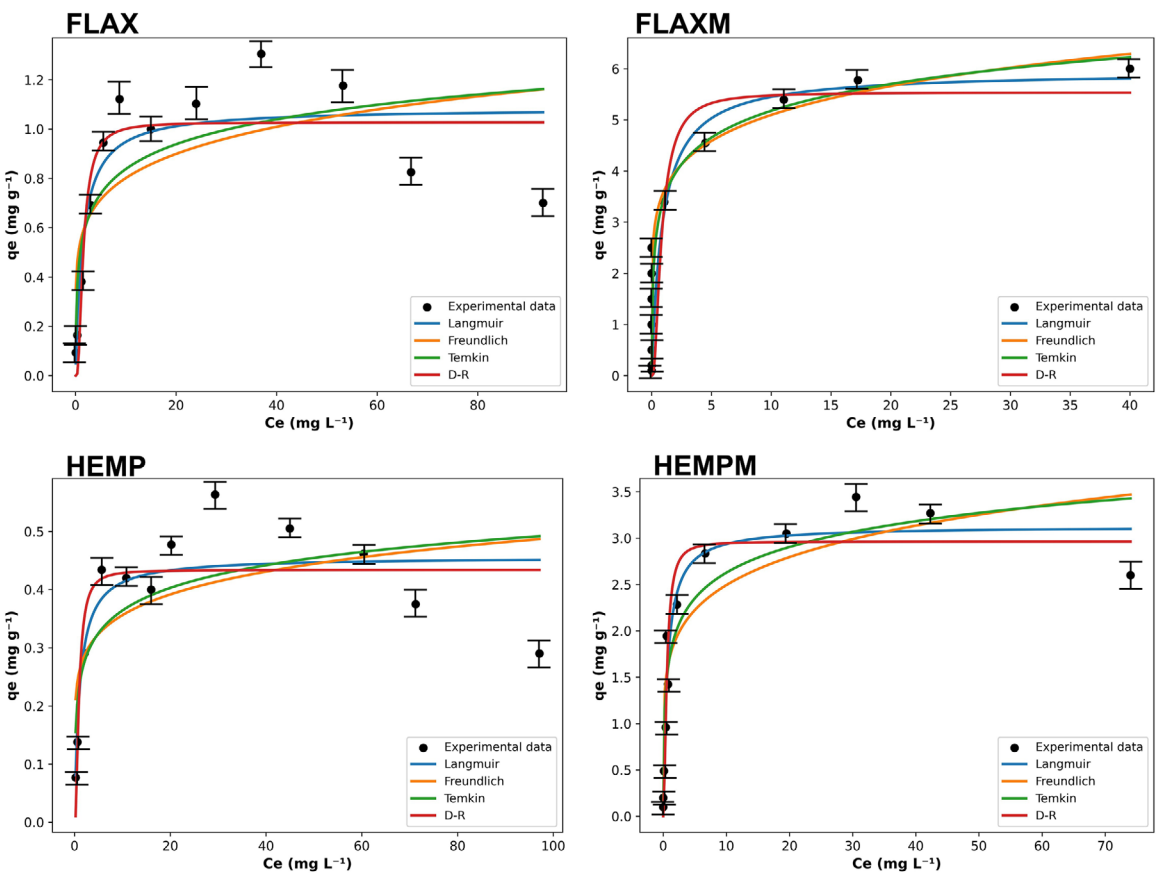

FIGURE 8 | Nonlinear isotherm fitting of Mn^{2+} adsorption onto native (HEMP, FLAX) and BTCA-modified (HEMPM, FLAXM) lignocellulosic felt. Experimental conditions: adsorbent dose = 1 g; pH = 5; contact time = 1 h; temperature = 22 ± 1°C; volume of solution = 0.1 L.

TABLE 3 | Isotherm parameters obtained from the nonlinear modeling of the Mn^{2+} adsorption through native lignocellulosic (HEMP, FLAX) and BTCA-modified (HEMPM, FLAXM) felts.

	Freundlich isotherm model				Langmuir isotherm model				Temkin isotherm model				Dubinin–Radushkevich isotherm model				
HEMP	K_F (L mg^{-1})	n	R^2	RMSE	K_L (L mg^{-1})	Q_0 (mg g^{-1})	R^2	RMSE	K_T (L mg^{-1})	q_T (mg g^{-1})	R^2	RMSE	K (mg L^{-1})	q_m (mg g^{-1})	E (kJ mol^{-1})	R^2	RMSE
	0.26	7.2	0.5	0.1	0.94	0.45	0.8	0.07	64	0.06	0.56	0.09	2.2×10^{-9}	0.43	15.2	0.75	0.07
HEMPM	K_F (L mg^{-1})	n	R^2	RMSE	K_L (L mg^{-1})	Q_0 (mg g^{-1})	R^2	RMSE	K_T (L mg^{-1})	q_T (mg g^{-1})	R^2	RMSE	K (mg L^{-1})	q_m (mg g^{-1})	E (kJ mol^{-1})	R^2	RMSE
	1.7	6.0	0.85	0.44	1.5	3.12	0.95	0.3	70.1	0.4	0.9	0.37	1.1×10^{-9}	3.0	21.6	0.92	0.32
FLAX	K_F (L mg^{-1})	n	R^2	RMSE	K_L (L mg^{-1})	Q_0 (mg g^{-1})	R^2	RMSE	K_T (L mg^{-1})	q_T (mg g^{-1})	R^2	RMSE	K (mg L^{-1})	q_m (mg g^{-1})	E (kJ mol^{-1})	R^2	RMSE
	0.54	6.0	0.54	0.26	0.7	1.1	0.81	0.2	31.0	0.15	0.7	0.2	4.8×10^{-9}	1.0	10.2	0.82	0.16
FLAXM	K_F (L mg^{-1})	n	R^2	RMSE	K_L (L mg^{-1})	Q_0 (mg g^{-1})	R^2	RMSE	K_T (L mg^{-1})	q_T (mg g^{-1})	R^2	RMSE	K (mg L^{-1})	q_m (mg g^{-1})	E (kJ mol^{-1})	R^2	RMSE
	3.6	6.6	0.94	1.1	1.1	6.0	0.92	1.1	93.0	0.8	0.98	1.1	1.9×10^{-9}	5.5	16.3	0.97	1.1

TABLE 4 | Comparison of Mn^{2+} biosorption performance of various low-cost biosorbents reported in the literature, including best-fitting isotherm models, maximum biosorption capacity (q_{max}), and removal efficiency. Experimental conditions may vary significantly among studies (e.g., pH, initial concentration, and adsorbent dosage), thus direct comparison should be interpreted with caution. The BTCA-modified flax felt developed in this study is included for comparison.

Biosorbent	Best fit isotherm	q_{MAX} (mg g^{-1})	%Removal	Contact time (min)	References
Phragmites australis (common reed)	Langmuir	6.3	99%	60	[56]
Beet pulp shreds	—	4.7–6.8	—	60	[57]
Corncob biomass (acid-treated)	Langmuir & Freundlich	7.9 (acid-treated) / 6.5 (raw)	—	30	[58]
Banana blossom peels (NaOH-treated)	Langmuir & Freundlich	—	98%	150	[59]
Nitric acid-functionalized rice husk (NT-RH)	Freundlich	—	95%	60	[60]
BTCA modified flax	Langmuir & Dubinin–Radushkevich	6.0-10.7	>99%	60	This study
Taro stem	Freundlich	18.2	>90%	60	[61]
Sawdust waste biomass	Langmuir	25.7	—	60	[62]
Modified orange peel (demethoxylated, Ca-cross-linked	Freundlich	29.7	94.8%	360	[63]
Tannic acid-tethered cellulose	Langmuir	32.2	99%	30	[64]

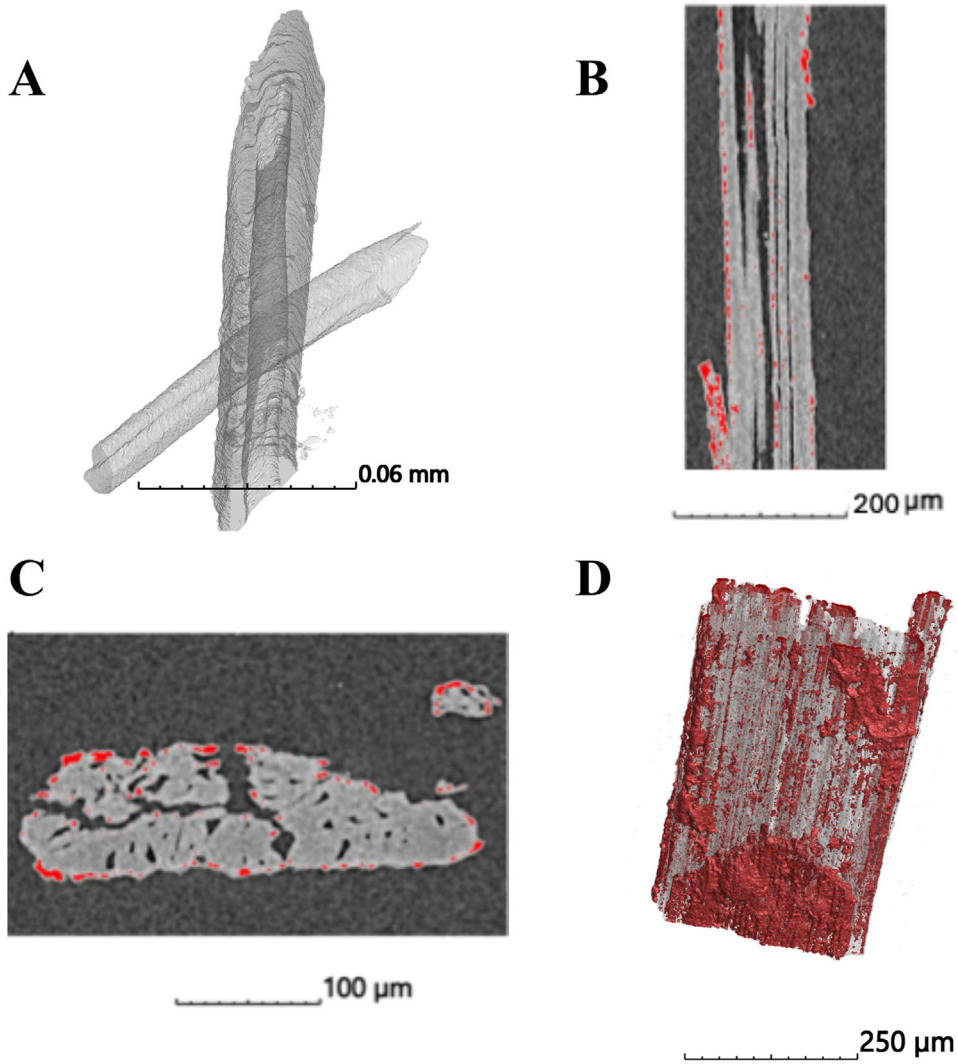

FIGURE 9 | Nanotomography images of a fiber extracted from the FLAXM sample before and after biosorption. (A) 3D reconstruction of the fiber prior to biosorption; (B) fiber image after biosorption along the longitudinal plane; (C) fiber image after biosorption along the transverse plane; (D) 3D reconstruction of the fiber after biosorption. High-intensity voxels corresponding to the metallic element Mn are shown in red.

high removal efficiencies. In this context, the BTCA-modified flax felt developed in the present study shows moderate biosorption performance (q_{max} = 6.0–10.7 mg g^{-1}), while still achieving excellent removal efficiency (>99%). This indicates that, although the maximum uptake is not among the highest reported, the material is highly effective under the tested conditions.

Importantly, the results highlight the role of surface functionalization in enhancing biosorption performance. Compared to untreated lignocellulosic felts, BTCA grafting significantly improves Mn^{2+} uptake through the introduction of carboxylic groups, promoting complexation mechanisms. Furthermore, the relatively simple preparation method and the use of renewable, low-cost precursors make these materials attractive for practical applications, particularly in decentralized or small-scale water treatment systems.

It is also worth noting that most of the studies reported in the literature identify the Langmuir model as the best-fitting isotherm, suggesting monolayer biosorption on relatively homogeneous surfaces. A similar trend was observed in the present work, especially for the BTCA-modified flax, further supporting the comparability of the biosorption mechanism with other biosorbents.

3 | Conclusion

This study demonstrated the suitability of lignocellulosic felts derived from hemp and flax, both in their native form and chemically modified through BTCA grafting, as effective biosorbents for Mn^{2+} removal from aqueous solutions. The batch experiments revealed that biosorption performance is strongly controlled by material composition, BTCA functionalization, and operating conditions such as pH, adsorbent dosage, and ionic strength.

Increasing the felt dosage enhanced Mn^{2+} uptake for all materials; however, BTCA-modified felts consistently outperformed their native counterparts, confirming the central role of carboxylate functionalities in metal complexation. Between the two

fiber types, flax displayed superior performance compared to hemp, both before and after modification. This improvement is attributable to flax's inherently higher α-cellulose content, finer fibers, and greater available surface area, which collectively favor BTCA anchoring and subsequent metal binding. These structural characteristics contribute to enhanced ion-exchange capacity, further explaining the higher Mn^{2+} removal observed for flax-based felts.

Solution pH was another decisive factor, particularly for BTCA-modified materials. The progressive deprotonation of BTCA carboxylic groups within the pH 3–6 range, consistent with their pKa values, enabled stronger electrostatic attraction and coordination of Mn^{2+}. Maximum removal was observed at pH values where the majority of –COOH groups shifted to -COO^-, confirming the complexation-driven mechanism. Conversely, low pH inhibited biosorption by suppressing carboxylate ionization and promoting competition between Mn^{2+} and H^+ ions for the same active sites.

The influence of ionic strength further supported this interpretation. The addition of NaCl (0.1–0.5 M) reduced Mn^{2+} uptake, particularly in BTCA-functionalized felts, due to competitive interactions between Na^+ and the -COO^- binding sites. Nevertheless, FLAXM and HEMPM maintained significantly higher removal efficiencies than unmodified materials even under saline conditions, demonstrating the robustness of BTCA-mediated complexation.

Isotherm modelling revealed that different biosorption mechanisms operate depending on the felt type. Native felts displayed moderate affinity, best described by the Langmuir model, suggesting monolayer adsorption onto relatively homogeneous sites. In contrast, FLAXM showed excellent agreement with Langmuir, Temkin, and D–R models and achieved Langmuir's maximum adsorption capacity (10.7 mg g^{-1}), over an order of magnitude greater than native flax. The mean free energy (greater than 18 kJ mol^{-1}), obtained through the D–R model, indicated a chemisorption mechanism consistent with coordination between Mn^{2+} and BTCA-derived carboxylate groups. Although chemisorption also appeared to dominate in the other felts, their weaker model fits prevented additional mechanistic detail.

Overall, these findings highlight the effectiveness of BTCA-modified flax felts as a promising, sustainable and low-cost material for Mn^{2+} removal from contaminated waters. Their high affinity, strong performance across variable conditions and clear chemisorption-driven behavior position them as particularly suitable candidates for industrial wastewater treatment applications. Future work should investigate regeneration, kinetic behavior and performance in real effluents to further support their practical implementation.

Acknowledgments

Grégorio Crini would like to thank the Université Marie et Louis Pasteur (Besançon, France) and the Région Bourgogne-Franche-Comté for funding this work under the CONFLANDEX 2025–2029 project, which allowed a Franco-Italian partnership to be established between the universities of Besançon and Bari, and to welcome Dario Lacalamita and Chiara Mongioví as visiting researchers in France. NMC and GC thank the PEA^2t analytical platform that manages the analytical equipment used in this study.

Conflicts of Interest

The author declares no conflicts of interest.

Data Availability Statement

The data that support the findings of this study are available from the corresponding author upon reasonable request.

References

1. P. M. Kohl and S. J. Medlar, *Occurrence of Manganese in Drinking Water and Manganese Control* (American Water Works Association, 2006).

2. B. I. Dvorak and B. Schuerman, "Drinking water: iron and manganese," (2021).

3. A. Postawa, C. Hayes, and A. Criscuoli, *Best Practice Guide on the Control of Iron and Manganese in Water Supply* (IWA Publishing, 2013), https://doi.org/10.2166/9781780400747.

4. Z. Zhang, C. Xiao, W. Yang, O. A. Adeyeye, and X. Liang, "Effects of the Natural Environment and Human Activities on Iron and Manganese Content in Groundwater: A Case Study of Changchun City, Northeast China," *Environmental Science and Pollution Research* 28 (2021): 41109–41119, https://doi.org/10.1007/s11356-021-13576-4.

5. H. Khozyem, A. Hamdan, A. A. Tantawy, A. Emam, and E. Elbadry, "Distribution and Origin of Iron and Manganese in Groundwater: Case Study, Balat-Teneida area, El-Dakhla Basin, Egypt," *Arabian Journal of Geosciences* 12 (2019): 523, https://doi.org/10.1007/s12517-019-4689-1.

6. M. S. Islam and M. Mostafa, "Occurrence, Source, and Mobilization of Iron, Manganese, and Arsenic Pollution in Shallow Aquifer," *Geofluids* 2023 (2023): 6628095, https://doi.org/10.1155/2023/6628095.

7. U. A. Usman, I. Yusoff, M. Raoov, et al., "Natural Sources of Iron and Manganese in Groundwater of the Lower Kelantan River Basin, North-Eastern Coast of Peninsula Malaysia: Water Quality Assessment and an Adsorption-Based Method for Remediation," *Environmental Earth Sciences* 80 (2021): 425, https://doi.org/10.1007/s12665-021-09717-0.

8. M. Wang, M. Wang, L. Yang, T. Yang, J. Li, and Y. Chen, "Distribution Characteristics and Genesis of Iron and Manganese Ions in Groundwater of Eastern Sanjiang Plain, China," *Water* 15 (2023): 2068, https://doi.org/10.3390/w15112068.

9. P. B. McMahon, K. Belitz, J. E. Reddy, and T. D. Johnson, "Elevated Manganese Concentrations in United States Groundwater, Role of Land Surface–Soil–Aquifer Connections," *Environmental Science & Technology* 53 (2018): 29–38, https://doi.org/10.1021/acs.est.8b04055.

10. M. Grohol and C. Veeh, "Study on the critical raw materials for the EU 2023," European Commission, Brussels (2023), https://doi.org/10.2873/725585.

11. E. Kalisińska and H. Budis, *Mammals and Birds as Bioindicators of Trace Element Contaminations in Terrestrial Environments: An Ecotoxicological Assessment of the Northern Hemisphere* (Springer Nature, 2019), 213–246, https://doi.org/10.1007/978-3-030-00121-6.

12. A. Mehri, "Trace Elements in Human Nutrition (II)—An Update," *International journal of preventive medicine* 11 (2020): 2, https://doi.org/10.4103/ijpvm.IJPVM_48_19.

13. E. Gumienna-Kontecka, M. Rowińska-Żyrek, and M. Łuczkowski, *Recent Advances in Trace Elements* (Wiley, 2018), 177–206, https://doi.org/10.1002/9781119133780.

14. World Health Organization, "Manganese in drinking water: background document for development of WHO guidelines for drinking water quality," (2021).

15. A. F. Rusydi, S.-I. Onodera, M. Saito, et al., "Vulnerability of Groundwater to Iron and Manganese Contamination in the Coastal Alluvial Plain of a Developing Indonesian City," *SN Applied Sciences* 3 (2021): 399, https://doi.org/10.1007/s42452-021-04385-y.

16. M. Gutierrez-Ruiz, J. F. Parrot, C. Ramirez-Nunez, L. Perez-Manzanera, D. Amaro-Ramirez, and L. Jardines-Mendoza, "Tridimensional Spatial Distribution of Manganese in a River Impacted by Metallurgical Activity and Mining," *Environmental Science and Pollution Research* 28 (2021): 3494–3505, https://doi.org/10.1007/s11356-020-10727-x.

17. A. A. Tinkov, M. M. B. Paoliello, A. N. Mazilina, et al., "Molecular Targets of Manganese-Induced Neurotoxicity: A Five-Year Update," *International Journal of Molecular Sciences* 22 (2021): 4246, https://doi.org/10.3390/ijms22094646.

18. M. Farina, D. S. Avila, J. B. da Rocha, and M. Aschner, "Metals, Oxidative Stress and Neurodegeneration: A Focus on Iron, Manganese and Mercury," *Neurochemistry International* 62 (2013): 575–594, https://doi.org/10.1016/j.neuint.2012.12.006.

19. M. A. Rahman, S. Kumar, D. Lamb, and M. M. Rahman, "Health Risk Assessment of Arsenic, Manganese, and Iron From Drinking Water for High School Children," *Water, Air, & Soil Pollution* 232 (2021): 269, https://doi.org/10.1007/s11270-021-05212-1.

20. Q. Wu, Q. Mu, Z. Xia, J. Min, and F. Wang, "Manganese Homeostasis at the Host-Pathogen Interface and in the Host Immune System," *Seminars in Cell & Developmental Biology* 115 (2021): 45–53, https://doi.org/10.1016/j.semcdb.2020.12.006.

21. M. Aschner and D. C. Dorman, "Manganese," *Toxicological Reviews* 25 (2006): 147–154, https://doi.org/10.2165/00139709-200625030-00002.

22. Agence Française de Sécurité des Aliments, "Assessment of the health risks from noncompliance with drinking water parametric values," (2004).

23. N. Morin-Crini, E. Lichtfouse, G. Liu, et al. in Emerging Contaminants Vol. 1, Vol. 65 (Eds.: N. Morin-Crini, E. Lichtfouse, G. Crini), Springer, Cham, 2021, pp. 1–46, https://doi.org/10.1007/978-3-030-69079-3_1.

24. A. Efligenir, S. Déon, P. Fievet, C. Druart, N. Morin-Crini, and G. Crini, "Decontamination of Polluted Discharge Waters From Surface Treatment Industries by Pressure-Driven Membranes: Removal Performances and Environmental Impact," *Chemical Engineering Journal* 258 (2014): 309–319, https://doi.org/10.1016/j.cej.2014.07.080.

25. D. Lacalamita, C. Mongioví, and G. Crini, "Chemical Substances Present in Discharge Water Generated by Laundry Industry: Analytical Monitoring," *Water Science and Engineering* 16 (2023): 324–332, https://doi.org/10.1016/j.wse.2023.07.004.

26. Q. Chen, Y. Yao, X. Li, J. Lu, J. Zhou, and Z. Huang, "Comparison of Heavy Metal Removals From Aqueous Solutions by Chemical Precipitation and Characteristics of Precipitates," *Journal of Water Process Engineering* 26 (2018): 289–300, https://doi.org/10.1016/j.jwpe.2018.11.003.

27. S. Bouarfa, E. Sauquet, T. Pelte, and M. Montginoul, "Comment partager l'eau en France?: à l'ère de l'anthropocène," (2025).

28. D. Legrand, *Annales Des Mines-Responsabilité & Environnement* (Institut Mines-Télécom, 2024), 20–26.

29. F. Galland, "L'eau," *Diplomatie* 137 (2026): 59–61.

30. A. Carrière, M. Brouillon, S. Sauvé, M. F. Bouchard, and B. Barbeau, "Performance of Point-of-Use Devices to Remove Manganese From Drinking Water," *Journal of Environmental Science and Health, Part A* 46 (2011): 601–607, https://doi.org/10.1080/10934529.2011.562852.

31. J. E. Tobiason, A. Bazilio, J. Goodwill, X. Mai, and C. Nguyen, "Manganese Removal From Drinking Water Sources," *Current Pollution Reports* 2 (2016): 168–177, https://doi.org/10.1007/s40726-016-0036-2.

32. M. Esskifati, Y. El Hammoudani, A. El Kasmi, and F. Dimane, *BIO Web of Conferences* (EDP Sciences, 2026), 01014, https://doi.org/10.1051/bioconf/202621201014.

33. C. Mongiovi, M. Jaillet, D. Lacalamita, et al., "A strategy to valorize a by-product of Pine Wood (Pinus Pinaster) for Copper removal from acqueous solutions," *Molecules* 28 (2023): 6436, https://doi.org/10.3390/molecules28186436.

34. C. Mongiovi, N. Morin-Crini, D. Lacalamita, et al., "Biosorbents From Plant Fibers of Hemp and Flax for Metal Removal: Comparison of Their Biosorption Properties," *Molecules* 26 (2021): 4199, https://doi.org/10.3390/molecules26144199.

35. C. Mongioví, N. Morin-Crini, V. Placet, et al., *Cannabis/Hemp for Sustainable Agriculture and Materials* (Springer Nature, 2022): 239–295, https://doi.org/10.1007/978-981-16-8778-5.

36. J. A. Okolie, S. Nanda, A. K. Dalai, and J. A. Kozinski, "Chemistry and Specialty Industrial Applications of Lignocellulosic Biomass," *Waste and Biomass Valorization* 12 (2021): 2145–2169, https://doi.org/10.1007/s12649-020-01123-0.

37. P. Saha, S. Chowdhury, D. Roy, B. Adhikari, J. K. Kim, and S. Thomas, "A brief Review on the Chemical Modifications of Lignocellulosic Fibers for Durable Engineering Composites," *Polymer Bulletin* 73 (2016): 587–620, https://doi.org/10.1007/s00289-015-1489-y.

38. R. Kozlowski, M. Wladyka-Przybylak, M. Helwig, and K. Kurzydłoski, "Composites Based on Lignocellulosic Raw Materials," *Molecular Crystals and Liquid Crystals* 418 (2004): 131–151, https://doi.org/10.1080/15421400490479217.

39. A. P. More, "Flax Fiber–Based Polymer Composites: A Review," *Advanced composites and hybrid materials* 5 (2022): 1–20, https://doi.org/10.1007/s42114-021-00246-9.

40. A. Moudood, A. Rahman, A. Öchsner, M. Islam, and G. Francucci, "Flax Fiber and Its Composites: An Overview of Water and Moisture Absorption Impact on Their Performance," *Journal of Reinforced Plastics and Composites* 38 (2019): 323–339, https://doi.org/10.1177/0731684418818893.

41. S. C. Das, A. D. La Rosa, S. Goutianos, and S. A. Grammatikos, *Plant Fibers, Their Composites, and Applications* (Elsevier, 2022), 209–232, https://doi.org/10.1016/B978-0-12-824528-6.00017-5.

42. A. Shahzad, "Hemp Fiber and Its Composites—A Review," *Journal of Composite Materials* 46 (2012): 973–986, https://doi.org/10.1177/0021998311413623.

43. M. Kostic, B. Pejic, and P. Skundric, "Quality of Chemically Modified Hemp Fibers," *Bioresource Technology* 99 (2008): 94–99, https://doi.org/10.1016/j.biortech.2006.11.050.

44. C. Q. Yang and Y. Xu, "Paper Wet Performance And Ester Crosslinking of Wood Pulp Cellulose by Poly (carboxylic acid) s," *Journal of Applied Polymer Science* 67 (1998): 649–658.

45. C. Q. Yang, Y. Xu, and D. Wang, "FT-IR Spectroscopy Study of the Polycarboxylic Acids Used for Paper Wet Strength Improvement," *Industrial & Engineering Chemistry Research* 35 (1996): 4037–4042, https://doi.org/10.1021/ie960207u.

46. V. A. Dehabadi, H.-J. Buschmann, and J. S. Gutmann, "Durable Press Finishing of Cotton Fabrics: An Overview," *Textile Research Journal* 83 (2013): 1974–1995, https://doi.org/10.1177/0040517513483857.

47. S. Loiacono, G. Crini, B. Martel, et al., "Simultaneous Removal of Cd, Co, Cu, Mn, Ni, and Zn From Synthetic Solutions on a Hemp-Based Felt. II. Chemical Modification," *Journal of Applied Polymer Science* 134 (2017): 45138, https://doi.org/10.1002/app.45138.

48. S. Amaducci, D. Scordia, F. Liu, et al., "Key Cultivation Techniques for Hemp in Europe and China," *Industrial Crops and Products* 68 (2015): 2–16, https://doi.org/10.1016/j.indcrop.2014.06.041.

49. J. Fromm, "Wood Formation of Trees in Relation To Potassium and Calcium Nutrition," *Tree Physiology* 30 (2010): 1140–1147, https://doi.org/10.1093/treephys/tpq024.

50. P. K. Hepler, "Calcium: A Central Regulator of Plant Growth and Development," *Plant Cell* 17 (2005): 2142–2155, https://doi.org/10.1105/tpc.105.032508.

51. J. Zhang, G. Henriksson, and G. Johansson, "Polygalacturonase is the Key Component in Enzymatic Retting of Flax," *Journal of Biotechnology* 81 (2000): 85–89, https://doi.org/10.1016/S0168-1656(00)00286-8.

52. M. Celus, C. Kyomugasho, A. M. Van Loey, T. Grauwet, and M. E. Hendrickx, "Influence of Pectin Structural Properties on Interactions With Divalent Cations and Its Associated Functionalities," *Comprehensive Reviews in Food Science and Food Safety* 17 (2018): 1576–1594, https://doi.org/10.1111/1541-4337.12394.

53. L. Ducoroy, B. Martel, M. Bacquet, and M. Morcellet, "Cation Exchange Finishing of Nonwoven Polyester With Polycarboxylic Acids and Cyclodextrins," *Journal of Applied Polymer Science* 103 (2007): 3730–3738, https://doi.org/10.1002/app.25249.

54. S. Sutheimer, M. Ferraco, and S. Cabaniss, "Molecular Size Effects on Carboxyl Acidity: Implications for Humic Substances," *Analytica Chimica Acta* 304 (1995): 187–194, https://doi.org/10.1016/0003-2670(94)00593-B.

55. B. Ji, P. Tang, K. Yan, and G. Sun, "Catalytic Actions of Alkaline Salts in Reactions Between 1,2,3,4-Butanetetracarboxylic Acid and Cellulose: II. Esterification," *Carbohydrate Polymers* 132 (2015): 228–236, https://doi.org/10.1016/j.carbpol.2015.06.070.

56. A. H. Mohammed, S. M. Shartooh, and M. Trigui, "Biosorption and Isotherm Modeling of Heavy Metals Using *Phragmites australis*," *Sustainability* 17 (2025): 5366, https://doi.org/10.3390/su17125366.

57. J. Chwastowski and P. Staroń, "Equilibrium, Kinetic and Thermodynamic Studies of Manganese Removal From Aqueous Solutions by Adsorption Process Using Beet Pulp Shreds as a Biosorbent," *Desalination and Water Treatment* 242 (2021): 117–127, https://doi.org/10.5004/dwt.2021.27844.

58. A. I. Adeogun, A. E. Ofudje, M. Idowu, and S. O. Kareem, "Equilibrium, Kinetic, and Thermodynamic Studies of the Biosorption of Mn (II) Ions From Aqueous Solution by Raw and Acid-Treated Corncob Biomass," *BioResources* 6 (2011): 4117–4134.

59. N. N. Rudi, N. Mohd Apandi, M. S. Muhamad, et al., "Chemical Treatment of Banana Blossom Peels Adsorbent as New Approach for Manganese Removal: Isotherm and Kinetic Studies," *Sustainability* 15 (2023): 10223, https://doi.org/10.3390/su151310223.

60. M. Hussain, A. S. Ali, T. Kousar, et al., "Efficient Removal of Manganese (II) Ions From Aqueous Solution Using Biosorbent Derived From Rice Husk," *Sustainable Chemistry One World* 5 (2025): 100047, https://doi.org/10.1016/j.scowo.2025.100047.

61. T. W. L. Xiao-ming, Z. R. L. Chun-li, and W. Yin-peng, "Batch Adsorption of Mn^{2+} From Aqueous Solution by Agricultural Waste Biomass Taro Stem," *Chinese Journal of Process Engineering* 11 (2011): 990.

62. F. Deniz, "Utilization of Sawdust Waste Biomass as an Eco-Friendly Biosorbent for Bioremediation of Manganese Pollution in Aqueous Environment," *Academic Perspective Procedia* 2 (2019): 823–830, https://doi.org/10.33793/acperpro.02.03.91.

63. L. Marzano-Vasquez, G. Torres-López, M. Baca-Neglia, et al., "Bioadsorption of Manganese With Modified Orange Peel in Aqueous Solution: Box–Behnken Design Optimization and Adsorption Isotherm," *Water* 17 (2025): 2152, https://doi.org/10.3390/w17142152.

64. A. Çalışır, S. Çağlar Yavuz, E. Yavuz, Ö. Arar, and M. Arda, "Removal of Manganese (Mn^{2+}) From Water Samples Using a Biocomposite Sorbent," *Environmental Research* 257 (2024): 119353, https://doi.org/10.1016/j.envres.2024.119353.

65. N. Morin-Crini, S. Loiacono, V. Placet, et al., "Hemp-Based Adsorbents for Sequestration of Metals: A Review," *Environmental Chemistry Letters* 17 (2019): 393–408, https://doi.org/10.1007/s10311-018-0812-x.

66. B. Martel, D. Ruffin, M. Weltrowski, Y. Lekchiri, and M. Morcellet, "Water-Soluble polymers and Gels From the Polycondensation Between Cyclodextrins and Poly(carboxylic acid)s: A Study of the Preparation Parameters," *Journal of Applied Polymer Science* 97 (2005): 433–442, https://doi.org/10.1002/app.21391.

67. C. Mongioví, G. Crini, X. Gabrion, et al., "Revealing the Adsorption Mechanism of Copper on Hemp-Based Materials Through EDX, Nano-CT, XPS, FTIR, Raman, and XANES Characterization Techniques," *Chemical Engineering Journal Advances* 10 (2022): 100282, https://doi.org/10.1016/j.ceja.2022.100282.

68. C. Mongioví, X. Gabrion, J. Govilas, et al., "Adsorption Location of Copper on Hemp Shives Revealed by Combination of K-Edge Subtraction X-Ray Micro-Tomography and X-Ray Micro-Fluorescence," *Cellulose* 31 (2024): 809–822, https://doi.org/10.1007/s10570-023-05685-9.

69. G. Crini, C. Bradu, C. Cosentino, et al., "Simultaneous Removal of Inorganic and Organic Pollutants From Polycontaminated Wastewaters on Modified Hemp-Based Felts," *Revista de Chimie* 72 (2021): 25–43, https://doi.org/10.37358/RC.21.1.8401.

70. B. T. Danat, R. A. Wuana, H. F. Chahul, and M. S. Iorungwa, "Review of Adsorption Isotherms Models," *Applied Water Science* 16 (2026): 72, https://doi.org/10.1007/s13201-025-02682-0.

71. J. Wang and X. Guo, "Adsorption Isotherm Models: Classification, Physical Meaning, Application and Solving Method," *Chemosphere* 258 (2020): 127279, https://doi.org/10.1016/j.chemosphere.2020.127279.

72. M. A. Al-Ghouti and D. A. Da'ana, "Guidelines for the Use and Interpretation of Adsorption Isotherm Models: A Review," *Journal of Hazardous Materials* 393 (2020): 122383, https://doi.org/10.1016/j.jhazmat.2020.122383.

73. N. Ayawei, A. N. Ebelegi, and D. Wankasi, "Modelling and Interpretation of Adsorption Isotherms," *Journal of Chemistry* 2017 (2017): 1–11, https://doi.org/10.1155/2017/3039817.

74. G. Crini, F. Gimbert, C. Robert, et al., "The removal of Basic Blue 3 From Aqueous Solutions by Chitosan-Based Adsorbent: Batch Studies," *Journal of Hazardous Materials* 153 (2008): 96–106, https://doi.org/10.1016/j.jhazmat.2007.08.025.

75. F. Renault, N. Morin-Crini, F. Gimbert, P. M. Badot, and G. Crini, "Cationized Starch-Based Material as a New Ion-Exchanger Adsorbent for the Removal of C.I. Acid Blue 25 From Aqueous Solutions," *Bioresource Technology* 99 (2008): 7573–7586, https://doi.org/10.1016/j.biortech.2008.02.011.

76. I. Langmuir, "The Adsorption of Gases on Plane Surfaces of Glass, Mica and Platinum," *Journal of the American Chemical Society* 40 (1918): 1361–1403, https://doi.org/10.1021/ja02242a004.

77. X. Guo and J. Wang, "Comparison of linearization Methods for Modeling the Langmuir Adsorption Isotherm," *Journal of Molecular Liquids* 296 (2019): 111850, https://doi.org/10.1016/j.molliq.2019.111850.

78. H. Freundlich, "Über die adsorption in lösungen," *Zeitschrift für Physikalische Chemie* 57 (1907), 385–470, https://doi.org/10.1515/zpch-1907-5723.

79. M. Temkin, "Kinetics of Ammonia Synthesis on Promoted Iron Catalysts," *Acta Physiochim URSS* 12 (1940): 327–356.

80. M. Dubinin, "The Equation of the Characteristic Curve of Activated Charcoal," *Doklady Akademii Nauk Sssr* 55 (1947): 327–329.

81. L. Liu, X.-B. Luo, L. Ding, and S.-L. Luo, *Nanomaterials for the Removal of Pollutants and Resource Reutilization* (Elsevier, 2019), 83–147.

82. K. H. Chu, "Revisiting the Temkin Isotherm: Dimensional Inconsistency and Approximate Forms," *Industrial & Engineering Chemistry Research* 60 (2021): 13140–13147, https://doi.org/10.1021/acs.iecr.1c01788.

83. K. H. Chu, M. A. Hashim, G. Hayder, and J.-C. Bollinger, "Comparative Evaluation of the Dubinin–Radushkevich Isotherm and Its Variants," *Industrial & Engineering Chemistry Research* 63 (2024): 15002–15011, https://doi.org/10.1021/acs.iecr.4c01895.

84. O. P. Murphy, M. Vashishtha, P. Palanisamy, and K. V. Kumar, "A Review on the Adsorption Isotherms and Design Calculations for the Optimization of Adsorbent Mass and Contact Time," *ACS Omega* 8 (2023): 17407–17430, https://doi.org/10.1021/acsomega.2c08155.

Supporting Information

Additional supporting information can be found online in the Supporting Information section.

The authors have cited additional references within the Supporting Information [65–84]. Materials and methods: materials and chemicals; grafting modifications of felts; scanning electron microscopy and energy x-ray analysis; computed nano-tomography analysis; nuclear magnetic resonance; ion exchange capacity; batch method for manganese biosorption; adsorption isotherm models. Grafted felts reutilization. Figure S1: Schematic illustration showing the possible reaction between 1,2,3,4-butanetetracarboxylic acid (BTCA) and anhydro-glucose units of two cellulose chains. Figure S2: EDX spectra of native (HEMP, FLAX) and BTCA-modified (HEMPM, FLAXM) lignocellulosic felts. Figure S3: NMR spectra of the BTCA-modified hemp felt (top) and native hemp felt (bottom). In the panel, the labeled carbons associated with their respective peaks are displayed. Figure S4. Percentage of manganese removal for different cycles of reutilization for modified flax and hemp felts.

Supporting File: slct73337-sup-0001-SuppMat.pdf.